AIAA-95-1729-CP

Optimum Aerodynamic Design Using CFD and Control Theory

Antony Jameson ‡
Department of Mechanical and Aerospace Engineering
Princeton University
Princeton, New Jersey, 08544 U.S.A.

Abstract

This paper describes the implementation of optimization techniques based on control theory for airfoil and wing design. The theory is applied to a system defined by the partial differential equations of the flow, with control by the boundary as a free surface. The Frechet derivative of the cost function is determined via the solution of an adjoint partial differential equation, and the boundary shape is then modified in a direction of descent. This process is repeated until an optimum solution is approached. Each design cycle requires the numerical solution of both the flow and the adjoint equations, leading to a computational cost roughly equal to the cost of two flow solutions. The cost is kept low by using multigrid techniques, which yield a sufficiently accurate solution in about 15 iterations. Satisfactory designs are usually obtained with 10-20 design cycles.

1 The Design Problem as a Control Problem

Aerodynamic design has traditionally been carried out on a cut and try basis, with the aerodynamic expertise of the designer guiding the selection of each shape modification. Although considerable gains in aerodynamic performance have been achieved by this approach, continued improvement will most probably be much more difficult to attain. The subtlety and complexity of fluid flow is such that it is unlikely that repeated trials in an interactive analysis and design procedure can lead to a truly optimum design. Automatic design techniques are therefore needed in order to fully realize the potential improvements in aerodynamic efficiency.

The simplest approach to optimization is to define the geometry through a set of design parameters, which may, for example, be the weights α_i applied to a set of shape functions $b_i(x)$ so that the shape is represented as

$$f(x) = \sum \alpha_i b_i(x).$$

Then a cost function I is selected which might, for example, be the drag coefficient or the lift to drag ratio, and I is regarded as a function of the parameters α_i. The sensitivities $\frac{\partial I}{\partial \alpha_i}$ may now be estimated by making a small variation $\delta\alpha_i$ in each design parameter in turn and recalculating the flow to obtain the change in I. Then

$$\frac{\partial I}{\partial \alpha_i} \approx \frac{I(\alpha_i + \delta\alpha_i) - I(\alpha_i)}{\delta\alpha_i}.$$

The gradient vector $\frac{\partial I}{\partial \alpha}$ may now be used to determine a direction of improvement. The simplest procedure is to make a step in the negative gradient direction by setting

$$\alpha^{n+1} = \alpha^n - \lambda\delta\alpha,$$

so that to first order

$$I + \delta I = I - \frac{\partial I^T}{\partial \alpha}\delta\alpha = I - \lambda\frac{\partial I^T}{\partial \alpha}\frac{\partial I}{\partial \alpha}.$$

More sophisticated search procedures may be used such as quasi-Newton methods, which attempt to estimate the second derivative $\frac{\partial^2 I}{\partial \alpha_i \partial \alpha_j}$ of the cost function from changes in the gradient $\frac{\partial I}{\partial \alpha}$ in successive optimization steps. These methods also generally introduce line searches to find the minimum in the search direction which is defined at each step. The main disadvantage of this approach is the need for a number of flow calculations proportional to the number of design variables to estimate the gradient. The computational costs can thus become prohibitive as the number of design variables is increased.

An alternative approach is to cast the design problem as a search for the shape that will generate the desired pressure distribution. This approach recognizes that the designer usually has an idea of the the kind of pressure distribution that will lead to the desired performance. Thus, it is useful to consider the inverse problem of calculating the shape that will lead to a given pressure distribution. The method has the advantage that only one flow solution is required to obtain the desired design. Unfortunately, a physically realizable shape may not necessarily exist, unless the pressure distribution satisfies certain constraints. Thus the problem must be very carefully formulated.

The problem of designing a two-dimensional profile to attain a desired pressure distribution was studied by Lighthill, who solved it for the case of incompressible flow with a conformal mapping of the profile to a unit circle [11]. The speed over the profile is

$$q = \frac{1}{h}\left|\nabla\phi\right|,$$

‡Professor, AIAA Fellow

where ϕ is the potential which is known for incompressible flow and h is the modulus of the mapping function. The surface value of h can be obtained by setting $q = q_d$, where q_d is the desired speed, and since the mapping function is analytic, it is uniquely determined by the value of h on the boundary. A solution exists for a given speed q_∞ at infinity only if

$$\frac{1}{2\pi}\oint q\, d\theta = q_\infty,$$

and there are additional constraints on q if the profile is required to be closed.

The difficulty that the target pressure may be unattainable may be circumvented by treating the inverse problem as a special case of the optimization problem, with a cost function which measures the error in the solution of the inverse problem. For example, if p_d is the desired surface pressure, one may take the cost function to be an integral over the the body surface of the square of the pressure error,

$$I = \frac{1}{2}\int_{\mathcal{B}} (p - p_d)^2 d\mathcal{B},$$

or possibly a more general Sobolev norm of the pressure error. This has the advantage of converting a possibly ill posed problem into a well posed one. It has the disadvantage that it incurs the computational costs associated with optimization procedures.

For some time the present author has advocated the advantages of formulating both the inverse problem and more general aerodynamic problems within the framework of the mathematical theory for the control of systems governed by partial differential equations [12]. A wing, for example, is a device to produce lift by controlling the flow, and its design can be regarded as a problem in the optimal control of the flow equations by variation of the shape of the boundary. If the boundary shape is regarded as arbitrary within some requirements of smoothness, then the full generality of shapes cannot be defined with a finite number of parameters, and one must use the concept of the Frechet derivative of the cost with respect to a function. Clearly, such a derivative cannot be determined directly by finite differences of the design parameters because there are now an infinite number of these. Using techniques of control theory, however, the gradient can be determined indirectly by solving an adjoint equation which has coefficients defined by the solution of the flow equations. The cost of solving the adjoint equation is comparable to that of solving the flow equations. Thus the gradient can be determined with roughly the computational costs of two flow solutions, independently of the number of design variables, which may be infinite if the boundary is regarded as a free surface.

For flow about an airfoil or wing, the aerodynamic properties which define the cost function are functions of the flow-field variables (w) and the physical location of the boundary, which may be represented by the function $\mathcal{F}$, say. Then

$$I = I(w, \mathcal{F}),$$

and a change in $\mathcal{F}$ results in a change

$$\delta I = \frac{\partial I^T}{\partial w}\delta w + \frac{\partial I^T}{\partial \mathcal{F}}\delta \mathcal{F}, \tag{1}$$

in the cost function. Using control theory, the governing equations of the flowfield are introduced as a constraint in such a way that the final expression for the gradient does not require reevaluation of the flowfield. In order to achieve this δw must be eliminated from (1). Suppose that the governing equation R which expresses the dependence of w and $\mathcal{F}$ within the flowfield domain D can be written as

$$R(w, \mathcal{F}) = 0. \tag{2}$$

Then δw is determined from the equation

$$\delta R = \left[\frac{\partial R}{\partial w}\right]\delta w + \left[\frac{\partial R}{\partial \mathcal{F}}\right]\delta \mathcal{F} = 0. \tag{3}$$

Next, introducing a Lagrange Multiplier ψ, we have

$$\begin{aligned}\delta I &= \frac{\partial I^T}{\partial w}\delta w + \frac{\partial I^T}{\partial \mathcal{F}}\delta \mathcal{F} - \psi^T\left(\left[\frac{\partial R}{\partial w}\right]\delta w + \left[\frac{\partial R}{\partial \mathcal{F}}\right]\delta \mathcal{F}\right)\\ &= \left\{\frac{\partial I^T}{\partial w} - \psi^T\left[\frac{\partial R}{\partial w}\right]\right\}\delta w + \left\{\frac{\partial I^T}{\partial \mathcal{F}} - \psi^T\left[\frac{\partial R}{\partial \mathcal{F}}\right]\right\}\delta \mathcal{F}.\end{aligned}$$

Choosing ψ to satisfy the adjoint equation

$$\left[\frac{\partial R}{\partial w}\right]^T \psi = \frac{\partial I}{\partial w} \tag{4}$$

the first term is eliminated, and we find that

$$\delta I = \mathcal{G}\delta \mathcal{F}, \tag{5}$$

where

$$\mathcal{G} = \frac{\partial I^T}{\partial \mathcal{F}} - \psi^T\left[\frac{\partial R}{\partial \mathcal{F}}\right].$$

The advantage is that (5) is independent of δw, with the result that the gradient of I with respect to an arbitrary number of design variables can be determined without the need for additional flow-field evaluations. In the case that (2) is a partial differential equation, the adjoint equation (4) is also a partial differential equation and appropriate boundary conditions must be determined.

After making a step in the negative gradient direction, the gradient can be recalculated and the process repeated to follow a path of steepest descent until a minimum is reached. In order to avoid violating constraints, such as a minimum acceptable wing thickness, the gradient may be projected into the allowable subspace within which the constraints are satisfied. In this way one can devise procedures which must necessarily converge at least to a local minimum, and which can be accelerated by the use of more sophisticated descent methods such as conjugate gradient or quasi-Newton algorithms. There is the possibility of more than one local minimum, but in any case the method will lead to an improvement over the original design. Furthermore, unlike the traditional inverse algorithms, any measure of performance can be used as the cost function.

In reference [7] the author derived the adjoint equations for transonic flows modelled by both the potential flow equation and the Euler equations. The theory was developed in terms of partial differential equations, leading to an adjoint partial differential equation. In order to obtain numerical solutions both the flow and the adjoint equations must be discretized. The control theory might be applied directly to the discrete flow equations which result from the numerical approximation of the flow equations by finite element, finite volume or finite difference procedures. This leads directly to a set of discrete adjoint equations with a matrix which is the transpose of the Jacobian matrix of the full set of discrete nonlinear flow equations.

On a three-dimensional mesh with indices i, j, k the individual adjoint equations may be derived by collecting together all the terms multiplied by the variation $\delta_{wi,j,k}$ of the discrete flow variable $w_{i,j,k}$. The resulting discrete adjoint equations represent a possible discretization of the adjoint partial differential equation. If these equations are solved exactly they can provide an exact gradient of the inexact cost function which results from the discretization of the flow equations. On the other hand any consistent discretization of the adjoint partial differential equation will yield the exact gradient in the limit as the mesh is refined. The trade-off between the complexity of the adjoint discretization, the accuracy of the resulting estimate of the gradient, and its impact on the computational cost to approach an optimum solution is a subject of ongoing research, as indeed also remains true for the discretization of the flow equations.

The true optimum shape belongs to an infinitely dimensional space of design parameters. One motivation for developing the theory for the partial differential equations of the flow is to provide an indication in principle of how such a solution could be approached if sufficient computational resources were available. Another motivation is that it highlights the possibility of generating ill posed formulations of the problem. For example, if one attempts to calculate the sensitivity of the pressure at a particular location to changes in the boundary shape, there is the possibility that a shape modification could cause a shock wave to pass over that location. Then the sensitivity could become unbounded. The movement of the shock, however, is continuous as the shape changes. Therefore a quantity such as the drag coefficient, which is determined by integrating the pressure over the surface, also depends continuously on the shape. The adjoint equation allows the sensitivity of the drag coefficient to be determined without the explicit evaluation of pressure sensitivities which would be ill posed.

The discrete adjoint equations, whether they are derived directly or by discretization of the adjoint partial differential equation, are linear. Therefore they could be solved by direct numerical inversion. In three-dimensional problems on a mesh with, say, n intervals in each coordinate direction, the number of unknowns is proportional to n^3 and the bandwidth to n^2. The complexity of direct inversion is proportional to the number of unknowns multiplied by the square of the bandwidth, resulting in a complexity proportional to n^7. The cost of direct inversion can thus become prohibitive as the mesh is refined, and it becomes more efficient to use iterative solution methods. Moreover, because of the similarity of the adjoint equations to the flow equations, the same iterative methods which have been proved to be efficient for the solution of the flow equations are efficient for the solution of the adjoint equations. This approach to optimal aerodynamics design has proved effective in a variety of applications [8, 10, 15]. The adjoint equations have also been used by Ta'asam, Kuruvila and Salas [16], who have implemented a one shot approach in which the constraint represented by the flow equations is only required to be satisfied by the final converged solution, and computational costs are also reduced by applying multigrid techniques to the geometry modifications as well as the solution of the flow and adjoint equations. Pironneau has studied the use of control theory for optimal shape design of systems governed by elliptic equations [13], and more recently the Navier-Stokes equations, and also wave reflection problems. Adjoint methods have also been used by Baysal and Eleshaky [1].

The next section presents the formulation for the case of airfoils in transonic flow. The governing equation is taken to be the transonic potential flow equation, and the profile is generated by conformal mapping from a unit circle. Thus the control is taken to be the modulus of the mapping function on the boundary. This leads to a generalization of Lighthill's method both to compressible flow, and to design for more general criteria. Numerical results are presented in Section 3. The mathematical development resembles, in certain respects, the method of calculating transonic potential flow developed by Bristeau, Pironneau, Glowinski, Periaux, Perrier and Poirier, who reformulated the solution of the flow equations as a least squares problem in control theory [2].

The subsequent sections discuss the application of the method to automatic wing design with the flow modelled by the three-dimensional Euler equations. The computational costs are low enough that it has proved possible to determine optimum wing designs in a few hours on workstations such as the IBM590 or the Silicon Graphics Power Indigo2.

2 Airfoil Design for Potential Flow using Conformal Mapping

Consider the case of two-dimensional compressible inviscid flow. In the absence of shock waves, an initially irrotational flow will remain irrotational, and we can assume that the velocity vector $\mathbf{q}$ is the gradient of a potential ϕ. In the presence of weak shock waves this remains a fairly good approximation.

Let p, ρ, c, and M be the pressure, density, speed-of-sound, and Mach number q/c. Then the potential flow equation is

$$\nabla \cdot (\rho \nabla \phi) = 0, \tag{6}$$

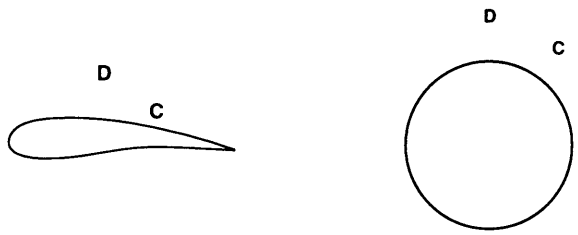

1a: z-Plane. 1b: σ-Plane.

Figure 1: Conformal Mapping.

where the density is given by

$$\rho = \left\{ 1 + \frac{\gamma - 1}{2} M_\infty^2 \left(1 - q^2\right) \right\}^{\frac{1}{(\gamma-1)}}, \tag{7}$$

while

$$p = \frac{\rho^\gamma}{\gamma M_\infty^2}, \quad c^2 = \frac{\gamma p}{\rho}. \tag{8}$$

Here M_∞ is the Mach number in the free stream, and the units have been chosen so that p and q have a value of unity in the far field.

Suppose that the domain D exterior to the profile C in the z-plane is conformally mapped on to the domain exterior to a unit circle in the σ-plane as sketched in Figure 1. Let R and θ be polar coordinates in the σ-plane, and let r be the inverted radial coordinate $\frac{1}{R}$. Also let h be the modulus of the derivative of the mapping function

$$h = \left| \frac{dz}{d\sigma} \right|. \tag{9}$$

Now the potential flow equation becomes

$$\frac{\partial}{\partial \theta} \left(\rho \phi_\theta \right) + r \frac{\partial}{\partial r} \left(r \rho \phi_r \right) = 0 \text{ in } D, \tag{10}$$

where the density is given by equation (7), and the circumferential and radial velocity components are

$$u = \frac{r \phi_\theta}{h}, \quad v = \frac{r^2 \phi_r}{h}, \tag{11}$$

while

$$q^2 = u^2 + v^2. \tag{12}$$

The condition of flow tangency leads to the Neumann boundary condition

$$v = \frac{1}{h} \frac{\partial \phi}{\partial r} = 0 \text{ on } C. \tag{13}$$

In the far field, the potential is given by an asymptotic estimate, leading to a Dirichlet boundary condition at $r = 0$ [3].

Suppose that it is desired to achieve a specified velocity distribution q_d on C. Introduce the cost function

$$I = \frac{1}{2} \int_C \left(q - q_d \right)^2 \, d\theta,$$

The design problem is now treated as a control problem where the control function is the mapping modulus h, which is to be chosen to minimize I subject to the constraints defined by the flow equations (6–13).

A modification δh to the mapping modulus will result in variations $\delta \phi$, δu, δv, and $\delta \rho$ to the potential, velocity components, and density. The resulting variation in the cost will be

$$\delta I = \int_C \left(q - q_d \right) \delta q \, d\theta, \tag{14}$$

where, on C, $q = u$. Also,

$$\delta u = r \frac{\delta \phi_\theta}{h} - u \frac{\delta h}{h}, \quad \delta v = r^2 \frac{\delta \phi_r}{h} - v \frac{\delta h}{h},$$

while according to equation (7)

$$\frac{\partial \rho}{\partial u} = -\frac{\rho u}{c^2}, \quad \frac{\partial \rho}{\partial v} = -\frac{\rho v}{c^2}.$$

It follows that $\delta \phi$ satisfies

$$L \delta \phi = -\frac{\partial}{\partial \theta} \left(\rho M^2 \phi_\theta \frac{\delta h}{h} \right) - r \frac{\partial}{\partial r} \left(\rho M^2 r \phi_r \frac{\delta h}{h} \right)$$

where

$$\begin{aligned} L \equiv & \frac{\partial}{\partial \theta} \left\{ \rho \left(1 - \frac{u^2}{c^2} \right) \frac{\partial}{\partial \theta} - \frac{\rho u v}{c^2} r \frac{\partial}{\partial r} \right\} \\ & + r \frac{\partial}{\partial r} \left\{ \rho \left(1 - \frac{v^2}{c^2} \right) r \frac{\partial}{\partial r} - \frac{\rho u v}{c^2} \frac{\partial}{\partial \theta} \right\}. \end{aligned} \tag{15}$$

Then, if ψ is any periodic differentiable function which vanishes in the far field,

$$\int_D \frac{\psi}{r^2} L \, \delta \phi \, dS = \int_D \rho M^2 \nabla \phi \cdot \nabla \psi \frac{\delta h}{h} \, dS, \tag{16}$$

where dS is the area element $r \, dr \, d\theta$, and the right hand side has been integrated by parts.

Now we can augment equation (14) by subtracting the constraint (16). The auxiliary function ψ then plays the role of a Lagrange multiplier. Thus,

$$\begin{aligned} \delta I = & \int_C \left(q - q_d \right) q \frac{\delta h}{h} \, d\theta - \int_C \delta \phi \frac{\partial}{\partial \theta} \left(\frac{q - q_d}{h} \right) d\theta \\ & - \int_D \frac{\psi}{r^2} L \delta \psi \, dS + \int_D \rho M^2 \nabla \phi \cdot \nabla \psi \frac{\delta h}{h} \, dS. \end{aligned}$$

Now suppose that ψ satisfies the adjoint equation

$$L \psi = 0 \text{ in } D \tag{17}$$

with the boundary condition

$$\frac{\partial \psi}{\partial r} = \frac{1}{\rho} \frac{\partial}{\partial \theta} \left(\frac{q - q_d}{h} \right) \text{ on } C. \tag{18}$$

Then, integrating by parts,

$$\int_D \frac{\psi}{r^2} L \delta \phi \, dS = -\int_C \rho \psi_r \delta \phi \, d\theta,$$

and

$$\begin{aligned} \delta I = & -\int_C \left(q - q_d \right) q \frac{\delta h}{h} \, d\theta \\ & + \int_D \rho M^2 \nabla \phi \cdot \nabla \psi \frac{\delta h}{h} \, dS. \end{aligned} \tag{19}$$

Here the first term represents the direct effect of the change in the metric, while the area integral represents a correction for the effect of compressibility. When the second term is deleted the method reduces to a variation of Lighthill's method [11].

Equation (19) can be further simplified to represent δI purely as a boundary integral because the mapping function is fully determined by the value of its modulus on the boundary. Set

$$\log \frac{dz}{d\sigma} = \mathcal{F} + i\beta,$$

where

$$\mathcal{F} = \log \left| \frac{dz}{d\sigma} \right| = \log h,$$

and

$$\delta \mathcal{F} = \frac{\delta h}{h}.$$

Then $\mathcal{F}$ satisfies Laplace's equation

$$\Delta \mathcal{F} = 0 \text{ in } D,$$

and if there is no stretching in the far field, $\mathcal{F} \to 0$. Also $\delta \mathcal{F}$ satisfies the same conditions. Introduce another auxiliary function P which satisfies

$$\Delta P = \rho M^2 \nabla \psi \cdot \nabla \psi \text{ in } D, \tag{20}$$

and

$$P = 0 \text{ on } C.$$

Then, the area integral in equation (19) is

$$\int_D \Delta P \, \delta \mathcal{F} \, dS = \int_C \delta \mathcal{F} \frac{\partial P}{\partial r} \, d\theta - \int_D P \Delta \, \delta \mathcal{F} \, dS,$$

and finally

$$\delta I = \int_C \mathcal{G} \, \delta \mathcal{F} \, d\theta,$$

where $\mathcal{F}_c$ is the boundary value of $\mathcal{F}$, and

$$\mathcal{G} = \frac{\partial P}{\partial r} - (q - q_d) \, q. \tag{21}$$

This suggests setting

$$\delta \mathcal{F}_c = -\lambda \mathcal{G}$$

so that if λ is a sufficiently small positive quantity

$$\delta I = -\int_C \lambda \mathcal{G}^2 \, d\theta < 0.$$

Arbitrary variations in $\mathcal{F}$ cannot, however, be admitted. The condition that $\mathcal{F} \to 0$ in the far field, and also the requirement that the profile should be closed, imply constraints which must be satisfied by $\mathcal{F}$ on the boundary C. Suppose that $\log \left(\frac{dz}{d\sigma} \right)$ is expanded as a power series

$$\log \left(\frac{dz}{d\sigma} \right) = \sum_{n=o}^{\infty} \frac{c_n}{\sigma^n}, \tag{22}$$

where only negative powers are retained, because otherwise $\left(\frac{dz}{d\sigma} \right)$ would become unbounded for large σ. The condition that $\mathcal{F} \to 0$ as $\sigma \to \infty$ implies

$$c_o = 0.$$

Also, the change in z on integration around a circuit is

$$\Delta z = \int \frac{dz}{d\sigma} \, d\sigma = 2\pi i \, c_1,$$

so the profile will be closed only if

$$c_1 = 0.$$

In order to satisfy these constraints, we can project $\mathcal{G}$ onto the admissible subspace for $\mathcal{F}_c$ by setting

$$c_o = c_1 = 0. \tag{23}$$

Then the projected gradient $\tilde{\mathcal{G}}$ is orthogonal to $\mathcal{G} - \tilde{\mathcal{G}}$, and if we take

$$\delta \mathcal{F}_c = -\lambda \tilde{\mathcal{G}},$$

it follows that to first order

$$\begin{aligned} \delta I &= -\int_C \lambda \mathcal{G} \tilde{\mathcal{G}} \, d\theta = -\int_C \lambda \left(\tilde{\mathcal{G}} + \mathcal{G} - \tilde{\mathcal{G}} \right) \mathcal{G} \, d\theta \\ &= -\int_C \lambda \tilde{\mathcal{G}}^2 \, d\theta < 0. \end{aligned}$$

If the flow is subsonic, this procedure should converge toward the desired speed distribution since the solution will remain smooth, and no unbounded derivatives will appear. If, however, the flow is transonic, one must allow for the appearance of shock waves in the trial solutions, even if q_d is smooth. Then $q - q_d$ is not differentiable. This difficulty can be circumvented by a more sophisticated choice of the cost function. Consider the choice

$$I = \frac{1}{2} \int_C \left(\lambda_1 \mathcal{Z}^2 + \lambda_2 \left(\frac{d\mathcal{Z}}{d\theta} \right)^2 \right) d\theta, \tag{24}$$

where λ_1 and λ_2 are parameters, and the periodic function $\mathcal{Z}(\theta)$ satisfies the equation

$$\lambda_1 \mathcal{Z} - \frac{d}{d\theta} \lambda_2 \frac{d\mathcal{Z}}{d\theta} = q - q_d. \tag{25}$$

Then,

$$\begin{aligned} \delta I &= \int_C \left(\lambda_1 \mathcal{Z} \, \delta \mathcal{Z} + \lambda_2 \frac{d\mathcal{Z}}{d\theta} \frac{d}{d\theta} \delta \mathcal{Z} \right) d\theta \\ &= \int_C \mathcal{Z} \left(\lambda_1 \, \delta \mathcal{Z} - \frac{d}{d\theta} \lambda_2 \frac{d}{d\theta} \delta \mathcal{Z} \right) d\theta = \int_C \mathcal{Z} \, \delta q \, d\theta. \end{aligned}$$

Thus, $\mathcal{Z}$ replaces $q - q_d$ in the previous formulas, and if one modifies the boundary condition (18) to

$$\frac{\partial \psi}{\partial r} = \frac{1}{\rho} \frac{\partial}{\partial \theta} \left(\frac{\mathcal{Z}}{h} \right) \text{ on } C, \tag{26}$$

the formula for the gradient becomes

$$\mathcal{G} = \frac{\partial P}{\partial r} - \mathcal{Z} q \tag{27}$$

instead of equation (21). Smoothing can also be introduced directly in the descent procedure by choosing $\delta\mathcal{F}_c$ to satisfy

$$\delta\mathcal{F}_c - \frac{\partial}{\partial\theta}\beta\frac{\partial}{\partial\theta}\delta\mathcal{F}_c = -\lambda\mathcal{G}, \tag{28}$$

where β is a smoothing parameter. Then to first order

$$\int \mathcal{G}\,\delta\mathcal{F} = -\frac{1}{\lambda}\int\left(\delta\mathcal{F}_c^2 - \delta\mathcal{F}_c\frac{\partial}{\partial\theta}\beta\frac{\partial}{\partial\theta}\delta\mathcal{F}_c\right)d\theta$$
$$= -\frac{1}{\lambda}\int\left(\delta\mathcal{F}_c^2 + \beta\left(\frac{\partial}{\partial\theta}\delta\mathcal{F}_c\right)^2\right)d\theta < 0.$$

The smoothed correction should now be projected onto the admissible subspace.

The final design procedure is thus as follows. Choose an initial profile and corresponding mapping function $\mathcal{F}$. Then:

1. Solve the flow equations (6–13) for ϕ, u, v, q, ρ.
2. Solve the ordinary differential equation (25) for $\mathcal{Z}$.
3. Solve the adjoint equation (15 and 17) or ψ subject to the boundary condition (26).
4. Solve the auxiliary Poisson equation (20) for P.
5. Evaluate $\mathcal{G}$ by equation (27)
6. Correct the boundary mapping function $\mathcal{F}_c$ by $\delta\mathcal{F}_c$ calculated from equation (28), projected onto the admissible subspace defined by (23).
7. Return to step 1.

3 Numerical Tests of Optimal Airfoil Design

The practical realization of the design procedure depends on the availability of sufficiently fast and accurate numerical procedures for the implementation of the essential steps, in particular the solution of both the flow and the adjoint equations. If the numerical procedures are not accurate enough, the resulting errors in the gradient may impair or prevent the convergence of the descent procedure. If the procedures are too slow, the cumulative computing time may become excessive. In this case, it was possible to build the design procedure around the author's computer program FLO36, which solves the transonic potential flow equation in conservation form in a domain mapped to the unit disk. The solution is obtained by a very rapid multigrid alternating direction method. The original scheme is described in Reference [4]. The program has been much improved since it was originally developed, and well converged solutions of transonic flows on a mesh with 128 cells in the circumferential direction and 32 cells in the radial direction are typically obtained in 5-20 multigrid cycles. The scheme uses artificial dissipative terms to introduce upwind biasing which simulates the rotated difference scheme [3], while preserving the conservation form. The alternating direction method is a generalization of conventional alternating direction methods, in which the scalar parameters are replaced by upwind difference operators to produce a scheme which remains stable when the type changes from elliptic to hyperbolic as the flow becomes locally supersonic [4]. The conformal mapping is generated by a power series of the form of equation (22) with an additional term

$$\left(1 - \frac{\epsilon}{\phi}\right)\log\left(1 - \frac{1}{\sigma}\right)$$

to allow for a wedge angle ϵ at the trailing edge. The coefficients are determined by an iterative process with the aid of fast Fourier transforms [3].

The adjoint equation has a form very similar to the flow equation. While it is linear in its dependent variable, it also changes type from elliptic in subsonic zones of the flow to hyperbolic in supersonic zones of the flow. Thus, it was possible to adapt exactly the same algorithm to solve both the adjoint and the flow equations, but with reverse biasing of the difference operators in the downwind direction in the adjoint equation, corresponding to the reversed direction of the zone of dependence. The Poisson equation (20) is solved by the Buneman algorithm.

The efficiency of the present approach, which uses separate discretizations of the flow and adjoint equations, depends on the fact that in the limit of zero mesh width the discrete adjoint solution converges to the true adjoint solution. This allows the use of a rather simple discretization of the adjoint equation modeled after the discretization of the flow equation. Numerical experiments confirm that in practice separate discretizations of the flow and adjoint equations yields good convergence to an optimum solution.

As an example of the application of the method, Figure 3 presents a calculation in which an airfoil was redesigned to improve its transonic performance by reducing the pressure drag induced by the appearance of a shock wave. The drag coefficient was therefore included in the cost function so that equation (24) is replaced by

$$I = \frac{1}{2}\int_C\left(\lambda_1\mathcal{Z}^2 + \lambda_2\left(\frac{d\mathcal{Z}}{d\theta}\right)^2\right)d\theta + \lambda_3 C_d,$$

where λ_3 is a parameter which may be varied to alter the trade-off between drag reduction and deviation from the desired pressure distribution. Representing the drag as

$$D = \int_C (p - p_\infty)\frac{dy}{d\theta}\,d\theta,$$

the procedure of Section 2 may be used to determine the gradient by solving the adjoint equation with a modified boundary condition. A penalty on the desired pressure distribution is still needed to avoid a situation in which the optimum shape is a flat plate with no lift and no drag.

It was also desired to preserve the subsonic characteristics of the airfoil. Therefore two design points were specified, Mach 0.20 and Mach 0.720, and in each case the lift coefficient was forced to be 0.6. The composite cost function was taken to be the sum of the values of

the cost function at the two design points. The transonic drag coefficient was reduced from 0.0191 to 0.0001 in 8 design cycles. In order to achieve this reduction the airfoil had to be modified so that its subsonic pressure distribution became more peaky at the leading edge. This is consistent with the results of experimental research on transonic airfoils, in which it has generally been found necessary to have a peaky subsonic presure distribution in order to delay the onset of the transonic drag rise. It is also important to control the adverse pressure gradient on the rear upper surface, which can lead to premature separation of the viscous boundary layer. It can be seen that there is no steepening of this gradient due to the redesign.

4 Three Dimensional Design using the Euler Equations

In order to illustrate further the application of control theory to aerodynamic design problems the next sections treat the case of three-dimensional wing design using the inviscid Euler equations as the mathematical model for compressible flow. In this case it proves convenient to denote the Cartesian coordinates and velocity components by x_1, x_2, x_3 and u_1, u_2, u_3, and to use the convention that summation over $i = 1$ to 3 is implied by a repeated index i. The three-dimensional Euler equations may be written as

$$\frac{\partial w}{\partial t} + \frac{\partial f_i}{\partial x_i} = 0 \quad \text{in } D, \tag{29}$$

where

$$w = \begin{Bmatrix} \rho \\ \rho u_1 \\ \rho u_2 \\ \rho u_3 \\ \rho E \end{Bmatrix}, \quad f_i = \begin{Bmatrix} \rho u_i \\ \rho u_i u_1 + p\delta_{i1} \\ \rho u_i u_2 + p\delta_{i2} \\ \rho u_i u_3 + p\delta_{i3} \\ \rho u_i H \end{Bmatrix} \tag{30}$$

and δ_{ij} is the Kronecker delta function. Also,

$$p = (\gamma - 1)\rho \left\{ E - \frac{1}{2}\left(u_i^2\right) \right\}, \tag{31}$$

and

$$\rho H = \rho E + p \tag{32}$$

where γ is the ratio of the specific heats. Consider a transformation to coordinates ξ_1, ξ_2, ξ_3 where

$$K_{ij} = \left[\frac{\partial x_i}{\partial \xi_j}\right], \quad J = \det(K), \quad K_{ij}^{-1} = \left[\frac{\partial \xi_i}{\partial x_j}\right].$$

Introduce contravariant velocity components as

$$\begin{Bmatrix} U_1 \\ U_2 \\ U_3 \end{Bmatrix} = K^{-1} \begin{Bmatrix} u_1 \\ u_2 \\ u_3 \end{Bmatrix}$$

The Euler equations can now be written as

$$\frac{\partial W}{\partial t} + \frac{\partial F_i}{\partial \xi_i} = 0 \quad \text{in } D, \tag{33}$$

with

$$W = J \begin{Bmatrix} \rho \\ \rho u_1 \\ \rho u_2 \\ \rho u_3 \\ \rho E \end{Bmatrix}, \quad F_i = J \begin{Bmatrix} \rho U_i \\ \rho U_i u_1 + \frac{\partial \xi_i}{\partial x_1} p \\ \rho U_i u_2 + \frac{\partial \xi_i}{\partial x_2} p \\ \rho U_i u_3 + \frac{\partial \xi_i}{\partial x_3} p \\ \rho U_i H \end{Bmatrix}. \tag{34}$$

Assume now that the new computational coordinate system conforms to the wing in such a way that the wing surface B_W is represented by $\xi_2 = 0$. Then the flow is determined as the steady state solution of equation (33) subject to the flow tangency condition

$$U_2 = 0 \quad \text{on } B_W. \tag{35}$$

At the far field boundary B_F, conditions are specified for incoming waves, as in the two-dimensional case, while outgoing waves are determined by the solution.

The weak form of the Euler equations for steady flow can be written as

$$\int_{\mathcal{D}} \frac{\partial \phi^T}{\partial \xi_i} F_i d\mathcal{D} = \int_{\mathcal{B}} n_i \phi^T F_i d\mathcal{B}, \tag{36}$$

where the test vector ϕ is an arbitrary differentiable function and n_i is the outward normal at the boundary. If a differentiable solution w is obtained to this equation, it can be integrated by parts to give

$$\int_{\mathcal{D}} \phi^T \frac{\partial F_i}{\partial \xi_i} d\mathcal{D} = 0$$

and since this is true for any ϕ, the differential form can be recovered. If the solution is discontinuous (36) may be integrated by parts separately on either side of the discontinuity to recover the shock jump conditions.

Suppose now that it is desired to control the surface pressure by varying the wing shape. It is convenient to retain a fixed computational domain. Variations in the shape then result in corresponding variations in the mapping derivatives defined by K. Introduce the cost function

$$I = \frac{1}{2} \iint_{B_W} (p - p_d)^2 \, d\xi_1 d\xi_3,$$

where p_d is the desired pressure. The design problem is now treated as a control problem where the control function is the wing shape, which is to be chosen to minimize I subject to the constraints defined by the flow equations (33–34). A variation in the shape will cause a variation δp in the pressure and consequently a variation in the cost function

$$\delta I = \iint_{B_W} (p - p_d)\, \delta p \;\; d\xi_1 d\xi_3. \tag{37}$$

Since p depends on w through the equation of state (31–32), the variation δp can be determined from the variation δw. Define the Jacobian matrices

$$A_i = \frac{\partial f_i}{\partial w}, \quad C_i = J K_{ij}^{-1} A_j. \tag{38}$$

The weak form of the equation for δw in the steady state becomes

$$\int_{\mathcal{D}} \frac{\partial \phi^T}{\partial \xi_i} \delta F_i d\mathcal{D} = \int_{\mathcal{B}} (n_i \phi^T \delta F_i) d\mathcal{B},$$

where

$$\delta F_i = C_i \delta w + \delta \left(J \frac{\partial \xi_i}{\partial x_j} \right) f_j,$$

which should hold for any differential test function ϕ. This equation may be added to the variation in the cost function, which may now be written as

$$\begin{aligned} \delta I = & \iint_{B_W} (p - p_d)\, \delta p \; d\xi_1 d\xi_3 \\ & - \int_{\mathcal{D}} \left(\frac{\partial \psi^T}{\partial \xi_i} \delta F_i \right) d\mathcal{D} \\ & + \int_{\mathcal{B}} \left(n_i \psi^T \delta F_i \right) d\mathcal{B}. \end{aligned} \tag{39}$$

On the wing surface B_W, $n_1 = n_3 = 0$ and it follows from equation (35) that

$$\delta F_2 = J \begin{Bmatrix} 0 \\ \frac{\partial \xi_2}{\partial x_1} \delta p \\ \frac{\partial \xi_2}{\partial x_2} \delta p \\ \frac{\partial \xi_2}{\partial x_3} \delta p \\ 0 \end{Bmatrix} + p \begin{Bmatrix} 0 \\ \delta \left(J \frac{\partial \xi_2}{\partial x_1} \right) \\ \delta \left(J \frac{\partial \xi_2}{\partial x_2} \right) \\ \delta \left(J \frac{\partial \xi_2}{\partial x_3} \right) \\ 0 \end{Bmatrix}. \tag{40}$$

Since the weak equation for δw should hold for an arbitrary choice of the test vector ϕ, we are free to choose ϕ to simplify the resulting expressions. Therefore we set $\phi = \psi$, where the costate vector ψ is the solution of the adjoint equation

$$\frac{\partial \psi}{\partial t} - C_i^T \frac{\partial \psi}{\partial \xi_i} = 0 \quad \text{in } D. \tag{41}$$

At the outer boundary incoming characteristics for ψ correspond to outgoing characteristics for δw. Consequently one can choose boundary conditions for ψ such that

$$n_i \psi^T C_i \delta w = 0.$$

Then if the coordinate transformation is such that $\delta \left(J K^{-1} \right)$ is negligible in the far field, the only remaining boundary term is

$$- \iint_{B_W} \psi^T \delta F_2 \; d\xi_1 d\xi_3.$$

Thus by letting ψ satisfy the boundary condition,

$$J \left(\psi_2 \frac{\partial \xi_2}{\partial x_1} + \psi_3 \frac{\partial \xi_2}{\partial x_2} + \psi_4 \frac{\partial \xi_2}{\partial x_3} \right) = (p - p_d) \quad \text{on } B_W, \tag{42}$$

we find finally that

$$\begin{aligned} \delta I = & - \int_{\mathcal{D}} \frac{\partial \psi^T}{\partial \xi_i} \delta \left(J \frac{\partial \xi_i}{\partial x_j} \right) f_j d\mathcal{D} \\ & - \iint_{B_W} \left\{ \psi_2 \frac{\partial \xi_2}{\partial x_1} + \psi_3 \frac{\partial \xi_2}{\partial x_2} + \psi_4 \frac{\partial \xi_2}{\partial x_3} \right\} p \, d\xi_1 d\xi_3. \end{aligned} \tag{43}$$

2a: x, y-Plane.

2b: ξ, η-Plane.

Figure 2: Sheared Parabolic Mapping:

A convenient way to treat a wing is to introduce sheared parabolic coordinates as shown in figure 2 through the transformation

$$\begin{aligned} x &= x_0(\zeta) + \frac{1}{2} a(\zeta) \left\{ \xi^2 - (\eta + \mathcal{S}(\xi, \zeta))^2 \right\} \\ y &= y_0(\zeta) + a(\zeta) \xi (\eta + \mathcal{S}(\xi, \zeta)) \\ z &= \zeta. \end{aligned}$$

Here $x = x_1$, $y = x_2$, $z = x_3$ are the Cartesian coordinates, and ξ and $\eta + \mathcal{S}$ correspond to parabolic coordinates generated by the mapping

$$x + iy = x_0 + iy_0 + \frac{1}{2} a(\zeta) \{ \xi + i(\eta + \mathcal{S}) \}^2$$

at a fixed span station ζ. $x_0(\zeta)$ and $y_0(\zeta)$ are the coordinates of a singular line which is swept to lie just inside the leading edge of a swept wing, while $a(\zeta)$ is a scale factor to allow for spanwise chord variations. The surface $\eta = 0$ is a shallow bump corresponding to the wing surface, with a height $\mathcal{S}(\xi, \zeta)$ determined by the equation

$$\xi + i\mathcal{S} = \sqrt{2 (x_{B_W} + i y_{B_W})},$$

where $x_{B_W}(z)$ and $y_{B_W}(z)$ are coordinates of points lying on the wing surface. We now treat $\mathcal{S}(\xi, \zeta)$ as the control.

In this case the transformation matrix $\left[\frac{\partial x_i}{\partial \xi_j} \right]$ becomes

$$\begin{aligned} K &= \begin{bmatrix} a(\xi - \tilde{\eta} \mathcal{S}_\xi) & -a\tilde{\eta} & \mathcal{A} - a\tilde{\eta}\mathcal{S}_\zeta \\ a(\tilde{\eta} + \xi \mathcal{S}_\xi) & a\xi & \mathcal{B} + a\xi \mathcal{S}_\zeta \\ 0 & 0 & 1 \end{bmatrix} \\ &= \begin{bmatrix} x_\xi & x_\eta & \mathcal{A} + x_\eta \mathcal{S}_\zeta \\ y_\xi & y_\eta & \mathcal{B} + y_\eta \mathcal{S}_\zeta \\ 0 & 0 & 1 \end{bmatrix}, \end{aligned}$$

where

$$\tilde{\eta} = (\eta + \mathcal{S}), \quad \mathcal{A} = a_\zeta \frac{x - x_0}{a} + x_{0_\zeta}, \quad \mathcal{B} = a_\zeta \frac{y - y_0}{a} + y_{0_\zeta}.$$

Now,

$$J = x_\xi y_\eta - x_\eta y_\xi = a^2 (\xi^2 + \tilde{\eta}^2)$$

and

$$J K^{-1} = \begin{bmatrix} y_\eta & -x_\eta & x_\eta \mathcal{B} - y_\eta \mathcal{A} \\ -y_\xi & x_\xi & y_\xi \mathcal{A} - x_\xi \mathcal{B} - J \mathcal{S}_\zeta \\ 0 & 0 & J \end{bmatrix}.$$

Then under a modification $\delta\mathcal{S}$

$$\begin{aligned}\delta x_\xi &= -a\left(\delta\mathcal{S}\mathcal{S}_\xi + \tilde{\eta}\delta\mathcal{S}_\xi\right)\\ \delta x_\eta &= -a\delta\mathcal{S}\\ \delta y_\xi &= a\left(\delta\mathcal{S} + \xi\delta\mathcal{S}_\xi\right)\\ \delta y_\eta &= 0.\end{aligned}$$

Thus

$$\delta J = 2a^2\tilde{\eta}\delta\mathcal{S}$$

and

$$\delta\left(J\,K^{-1}\right) = \begin{bmatrix} 0 & a\delta\mathcal{S} & -a\mathcal{B}\delta\mathcal{S} \\ -\delta y_\xi & \delta x_\xi & \mathcal{D} \\ 0 & 0 & \delta J \end{bmatrix}.$$

where

$$\mathcal{D} = \delta y_\xi\mathcal{A} - \delta x_\xi\mathcal{B} - a_\zeta\frac{J}{a}\delta\mathcal{S} - \delta J\mathcal{S}_\zeta - J\delta\mathcal{S}_z.$$

Inserting these formulas in equation (43) we find that the volume integral in δI is

$$\begin{aligned}&-\iiint\frac{\partial\psi^T}{\partial\xi}\delta\mathcal{S}a\left(f_2-\mathcal{B}f_3\right)\,d\xi\,d\eta\,d\zeta\\ &-\iiint\frac{\partial\psi^T}{\partial\eta}\left\{-\delta y_\xi f_1+\delta x_\xi f_2+\mathcal{D}f_3\right\}d\xi\,d\eta\,d\zeta\\ &-\iiint\frac{\partial\psi^T}{\partial\zeta}\delta J f_3\,d\xi\,d\eta\,d\zeta,\end{aligned}$$

where $\mathcal{S}$ and $\delta\mathcal{S}$ are independent of η. Therefore, integrating over η, the variation in the cost function can be reduced to a surface integral of the form

$$\delta I = \iint_{B_W}\left(P\left(\xi,\zeta\right)\delta\mathcal{S} - Q\left(\xi,\zeta\right)\delta\mathcal{S}_\xi - R\left(\xi,\zeta\right)\delta\mathcal{S}_\zeta\right)d\xi\,d\zeta$$

Here

$$\begin{aligned}P &= a\left(\psi_2+\mathcal{S}_\xi\psi_3+\mathcal{C}\psi_4\right)p\\ &-\int\frac{\partial\psi^T}{\partial\xi}a\left(f_2-\mathcal{B}f_3\right)d\eta\\ &+\int\frac{\partial\psi^T}{\partial\eta}a\left(f_1+\mathcal{S}_\xi f_2+\mathcal{C}\psi_3\right)d\eta\\ &-2\int\frac{\partial\psi^T}{\partial\zeta}a^2\tilde{\eta}d\eta\\ Q &= -a\left\{\xi\psi_2+\tilde{\eta}\psi_3-\left(\mathcal{A}\xi+\mathcal{B}\tilde{\eta}\right)\psi_4\right\}p\\ &-\int\frac{\partial\psi^T}{\partial\eta}a\left\{\xi f_1+\tilde{\eta}f_2-\left(\mathcal{A}\xi+\mathcal{B}\tilde{\eta}\right)f_3\right\}d\eta\\ R &= -J\psi_4 p\\ &-\int\frac{\partial\psi^T}{\partial\eta}Jf_3 d\eta,\end{aligned}$$

where

$$\mathcal{C} = 2a\tilde{\eta}\mathcal{S}_\zeta - \mathcal{A} - \mathcal{B}\mathcal{S}_\xi + a_\zeta\frac{J}{a^2}.$$

Also the shape change will be confined to a boundary region of the $\xi-\zeta$ plane, so we can integrate by parts to obtain

$$\delta I = \iint_{B_W}\left(P+\frac{\partial Q}{\partial\xi}+\frac{\partial R}{\partial\zeta}\right)\delta\mathcal{S}\;\,d\xi\,d\zeta.$$

Thus to reduce I we can choose

$$\delta\mathcal{S} = -\lambda\left(P+\frac{\partial Q}{\partial\xi}+\frac{\partial R}{\partial\zeta}\right),$$

where λ is sufficiently small and non-negative.

In order to impose a thickness constraint we can define a baseline surface $\mathcal{S}_0\left(\xi,\zeta\right)$ below which $\mathcal{S}\left(\xi,\zeta\right)$ is not allowed to fall. Now if we take $\lambda = \lambda\left(\xi,\zeta\right)$ as a non-negative function such that

$$\mathcal{S}\left(\xi,\zeta\right) + \delta\mathcal{S}\left(\xi,\zeta\right) \geq \mathcal{S}_0\left(\xi,\zeta\right).$$

Then the constraint is satisfied, while

$$\delta I = -\iint_{B_W}\lambda\left(P+\frac{\partial Q}{\partial\xi}+\frac{\partial R}{\partial\zeta}\right)^2 d\xi\,d\zeta \leq 0.$$

As in the case of design using a potential flow model, it is crucially important to introduce appropriate smoothing procedures. In order to avoid discontinuities in the adjoint boundary condition which would be caused by the appearance of shock waves, the cost function for the target pressure may be modified to the form

$$\begin{aligned}I &= \frac{1}{2}\iint\left(\lambda_1\mathcal{Z}+\lambda_2\left(\frac{\partial\mathcal{Z}}{\partial\xi}\right)^2\right)d\xi d\eta\\ \lambda_1\mathcal{Z} &- \frac{\partial}{\partial\xi}\lambda_2\frac{\partial\mathcal{Z}}{\partial\xi} = p - p_d.\end{aligned}$$

Then

$$\begin{aligned}\delta I &= \iint\left(\lambda_1\mathcal{Z}\delta\mathcal{Z}+\lambda_2\frac{\partial\mathcal{Z}}{\partial\xi}\frac{\partial}{\partial\xi}\delta\mathcal{Z}\right)d\xi d\eta\\ &= \iint\mathcal{Z}\left(\lambda_1-\frac{\partial}{\partial\xi}\lambda_2\frac{\partial}{\partial\xi}\right)\delta\mathcal{Z}\,d\xi d\eta\\ &= \iint\mathcal{Z}\delta p\,d\xi d\eta\end{aligned}$$

and the smooth quantity $\mathcal{Z}$ replaces $p-p_d$ in the adjoint boundary condition.

Independent movement of the boundary mesh points could produce discontinuities in the designed shape. In order to prevent this the gradient may be also smoothed. Both explicit and implicit smoothing procedures are useful. Suppose that the movement of the surface mesh points were defined by local B-splines. In the case of a uniform one-dimensional mesh, a B-spline with a displacement d centered at the mesh point i would produce displacements $d/4$ at $i+1$ and $i-1$ and zero elsewhere, while preserving continuity of the first and second derivatives. Thus we can suppose that the discrete surface displacement has the form

$$\delta S = Bd,$$

where B is a matrix with coefficients defined by the B-splines, and d_i is the displacement associated with the B-spline centered at i. Then, using the discrete formulas, to first order the change in the cost is

$$\delta I = \mathcal{G}^T\delta S = \mathcal{G}^T Bd.$$

Thus the gradient with respect to the B-spline coefficients is obtained by multiplying $\mathcal{G}$ by B^T, and a descent step is defined by setting

$$d = -\lambda B^T \mathcal{G},\ \delta S = Bd = -\lambda B B^T \mathcal{G}$$

where λ is sufficiently small and positive. The coefficients of B can be renormalized to produce unit row sums. With a uniform mesh spacing in the computational domain this formula is equivalent to the use of a gradient modified by two passes of the explicit smoothing procedure

$$\bar{\mathcal{G}}_{i,k} = \frac{1}{6}\mathcal{G}_{i-1,k} + \frac{2}{3}\mathcal{G}_{i,k} + \frac{1}{6}\mathcal{G}_{i+1,k}$$

with a similar smoothing procedure in the k discretization.

Implicit smoothing may also be used. The smoothing equation

$$-\epsilon_{i+\frac{1}{2},k}(\bar{\mathcal{G}}_{i+1,k} - \bar{\mathcal{G}}_{i,k}) + \epsilon_{i-\frac{1}{2},k}(\bar{\mathcal{G}}_{i,k} - \bar{\mathcal{G}}_{i-1,k}) = \mathcal{G}_{i,k}$$

approximates the differential equation

$$\bar{\mathcal{G}} - \frac{\partial}{\partial \xi}\epsilon\frac{\partial \bar{\mathcal{G}}}{\partial \xi} = \mathcal{G}$$

If one sets $\delta S = -\lambda \bar{\mathcal{G}}$, then to first order the change in the cost is

$$\begin{aligned}
\delta I &= -\int\int \mathcal{G}\delta S \, d\xi d\eta \\
&= -\frac{1}{\lambda}\int\int \left(\bar{\mathcal{G}} - \frac{\partial}{\partial \xi}\epsilon\frac{\partial \bar{\mathcal{G}}}{\partial \xi}\right)\bar{\mathcal{G}}\, d\xi d\eta \\
&= -\frac{1}{\lambda}\int\int \left(\bar{\mathcal{G}}^2 + \epsilon\left(\frac{\partial \bar{\mathcal{G}}}{\partial \xi}\right)^2\right) d\xi d\eta \\
&< 0,
\end{aligned}$$

assuring an improvement if λ is sufficiently small and positive, unless the process has already reached a stationary point at which $\mathcal{G} = 0$.

5 Implementation for Swept Wings

Since three dimensional calculations require substantial computational resources, it is extremely important for the practical implementation of the method to use fast solution algorithms for the flow and the adjoint equations. In this case the author's FLO87 computer program has been used as the basis of the design method. FLO87 solves the three dimensional Euler equations with a cell-centered finite volume scheme, and uses residual averaging and multigrid acceleration to obtain very rapid steady state solutions, usually in 25 to 50 multigrid cycles [5, 6]. Upwind biasing is used to produce nonoscillatory solutions, and assure the clean capture of shock waves. This is introduced through the addition of carefully controlled numerical diffusion terms, with a magnitude of order Δx^3 in smooth parts of the flow. The adjoint equations are treated in the same way as the flow equations. The fluxes are first estimated by central differences, and then modified by downwind biasing through numerical diffusive terms which are supplied by the same subroutines that were used for the flow equations.

The method has been tested for the optimization of several swept wings. In every case, the wing planform was fixed while the sections were free to be changed arbitrarily by the design method, with a restriction on the minimum thickness. The initial wing has a unit-semi-span, with 38 degrees leading edge sweep. It has a modified trapezoidal planform, with straight taper from a root chord of 0.38, and a curved trailing edge in the inboard region blending into straight taper outboard of the 30 percent span station to a tip chord of 0.10, with an aspect ratio of 9.0. The initial wing sections were based on a section specifically designed by the author's two dimensional design method [8] to give shock free flow at Mach 0.78 with a lift coefficient of 0.6. The pressure distribution is displayed in figure 4. This section, which has a thickness to chord ratio of 9.5 percent, was used at the tip. Similar sections with an increased thickness were used inboard. The variation of thickness was non-linear with a more rapid increase near the root, where the thickness to chord ratio of the basic section was multiplied by a factor of 1.47. The inboard sections were rotated upwards to give the initial wing 3.0 degrees twist from root to tip. The two-dimensional pressure distribution of the basic wing section at its design point was introduced as a target pressure distribution uniformly across the span. This target is presumably not realizable, but serves to favor the establishment of relatively benign pressure distribution. The total inviscid drag coefficient, due to the combination of vortex and shock wave drag, was also included in the cost function. The calculations were performed with the lift coefficient forced to approach a fixed value by adjusting the angle of attack every fifth iteration of the flow solution. It was found that the computational costs can be reduced by using only 15 multigrid cycles in each flow solution, and in each adjoint solution. Although this is not enough for full convergence, it proves sufficient to provide a shape modification which leads to an improvement.

Figures 5 and 6 show the result of a calculation at Mach number of 0.85, with the lift coefficient forced to approach a value of 0.5. This calculation was performed on a mesh with 192 intervals in the ξ direction wrapping around the wing, 32 intervals in the normal η direction and 48 intervals in the spanwise ζ direction, giving a total of 294912 cells. The wing was specified by 33 sections, each with 128 points, giving a total of 4224 design variables. The plots show the initial wing geometry and pressure distribution, and the modified geometry and pressure distribution after 40 design cycles. The total inviscid drag coefficient was reduced from 0.0207 to 0.0113. The initial design exhibits a very strong shock wave in the inboard region. It can be seen that this is completely eliminated, leaving a very weak shock wave in the outboard region. To verify the solution, the final geometry was analyzed with another method, using the computer program FLO67. This program uses a

cell-vertex formulation, and has recently been modified to incorporate a local extremum diminishing algorithm with a very low level of numerical diffusion [9]. When run to full convergence it was found that a better estimate of the drag coefficient of the redesigned wing is 0.0094 at Mach 0.85 with a lift coefficient of 0.5, giving a lift to drag ratio of 53. The result is illustrated in Figure 7. A calculation at Mach 0.500 shows a drag coefficient of 0.0087 for a lift coefficient of 0.5. Since in this case the flow is entirely subsonic, this provides an estimate of the vortex drag for this planform and lift distribution, which is just what one obtains from the standard formula for induced drag, $C_D = {C_L}^2/\epsilon\pi AR$, with an aspect ratio $AR = 9$, and an efficiency factor $\epsilon = 0.97$. Thus the design method has reduced the shock wave drag coefficient to about 0.0007 at a lift coefficient of 0.5.

Figures 8 and 9 show the result of another optimization starting from the same initial geometry, and at the same mach number of 0.850, but with the lift coefficient increased to 0.55. This produces stronger shock waves and is therefore a more severe test of the method. In this case the total inviscid drag coefficient was reduced from 0.0241 to 0.0136 in 48 design cycles. Again the performance of the final design was verified by a calculation with FLO67, using a high resolution LED algorithm, and when the result was fully converged the drag coefficient was found to be 0.0115. The result is illustrated in figure 10. A subsonic calculation at Mach .500 shows a drag coefficient of 0.0108 for a lift coefficient of 0.55. Thus in this case the shock wave drag coefficient is about 0.0007.

For a representative transport aircraft the parasite drag coefficient of the wing due to skin friction is about 0.0045. Also the fuselage drag coefficient is about 0.0050, the nacelle drag coefficient is about 0.0015, the empennage drag coefficient is about 0.0020, and excrescence drag coefficient is about 0.0010. This would give a total drag coefficient $C_D = 0.0255$ for a lift coefficient of 0.55, corresponding to a lift to drag ratio $L/D = 21.6$. This would be a substantial improvement over the values obtained by currently flying transport aircraft.

As another test of the method an initial wing was defined with the same planform and sections derived from the RAE 5225 airfoil. This airfoil is unusually thick for a super-critical design, with a thickness to chord ratio of 14%. The initial section at the mid-span point was an unmodified RAE 5225 profile. To allow margin for the optimization procedure to reduce the thickness of the inboard sections, the root thickness was multiplied by a factor of 1.16, while the tip thickness was reduced by a factor of 0.90. The inboard sections of the wing were again rotated upwards to give the initial wing a twist of 3 degrees from root to tip. In this case the optimization reduced the drag coefficient from 0.0253 to 0.0118 in 48 cycles. The results of the design calculation are shown in figures 11 and 12. It can be seen that the final wing still has fairly thick sections across the entire span. A fully converged calculation with FLO67, using a high resolution LED algorithm, indicates that a more accurate estimate of the drag coefficient of the final design is 0.0099 at a lift coefficient of 0.50. The results of this calculation is shown in figure 13. It may well pay to accept a shock drag penalty in the range of 0.0005 in order to increase the thickness of the wing section. This in turn could allow the use of a higher aspect ratio wing with the same structural weight, which might produce a larger saving in vortex drag than the penalty in shock drag.

In all of these tests the optimization procedure generated low drag wings in about $10 - 20$ design cycles, with very weak shock waves. Additional cycles were needed to drive the solution towards a shock free flow over most of the wing. The final designs, which are almost shock free, consistently exhibit pressure distributions with fairly strong leading edge suction peaks followed by a steady and gradual recompression. When these flows were analyzed by FLO67 to verify their properties, it was found that very complex wave patterns appear during the early evolution of the flow. These are finally eliminated as the flow reaches a steady state, but this process takes much longer than the evolution of the more usual type of flow with well established shock waves at the exit of the supersonic zone. The drag penalty incurred by designs with flat-topped pressure distributions and weak shock waves is very small. These designs , which can be produced with a much smaller number of optimization cycles, might be preferred in practice. The pressure distribution might then be tailored to move the suction peak downstream in order to delay the transition of the boundary layer to turbulent flow. In any case, one might wish to modify the inboard region of the existing designs to reduce the adverse pressure gradient at the trailing edge, which might otherwise be strong enough to induce separation.

6 Conclusion

In the period since this approach to optimal shape design was first proposed by the author [7], the method has been verified by numerical implementation for both potential flow and flows modeled by the Euler equations. It has been demonstrated that it can be successfully used with a finite volume formulation to perform calculations with arbitrary numerically generated grids [14]. The first results which have been obtained for swept wings with the three-dimensional Euler equations suggest that the method has now matured to the point where it can be a very useful tool for the design of new airplanes. Even in the case of three dimensional flows, the computational requirements are so moderate that the calculations can be performed with workstations such as the IBM RISC 6000 series. A design cycle on a 192x32x48 mesh takes about 20 minutes on an IBM model 590 workstation, allowing overnight completion of a design calculation for a swept wing.

The author is working with several collaborators both to improve the method and to extend it to a broader range of applications. In order to treat more complex geometries the method must be modified to accommodate

arbitrary meshes. In order to do this one can modify the initial mesh, which may be produced by a numerical grid generation procedure, by analytically defined grid perturbations which depend smoothly on modifications of the boundary shape. J. Reuther has implemented this procedure, and preliminary results for wing-body combinations are presented in [15]. The method has also been recently used to assist the design of a wing for a business jet. In order to apply the method to flows modelled by the Navier-Stokes equations the adjoint equations must be augmented by additional terms which corresponds to the viscous stresses in the momentum equations and viscous dissipation in the energy equation. Computer programs which implement these extensions for both two and three dimensional flows are currently being tested.

In order to further reduce the computational cost the author has collaborated with J. Alonso in the modification of the three dimensional Euler design code to run on parallel computers. Message passing is implemented with MPI. Preliminary timing results have been obtained for the IBM SP2. A design cycle on a mesh with 294912 cells requires about 63 seconds with 16 processors, or 42 seconds with 32 processors. A complete swept wing design using 12 design cycles can then be completed in 15 minutes with 16 processors, or in 10 minutes with 32 processors. The integrals needed to determine the gradient from the solution of the adjoint equation are evaluated on a single processor. This becomes a significant fraction of the total time when the number of processors exceeds 32, and this part of the process will also need to be performed in parallel to approach more closely to a linear speedup with a large number of processors. Parallel implementation is likely to be particularly important for design using the Navier-Stokes equations, for which much finer meshes are needed to assure sufficient accuracy, with a corresponding increase in the computational cost.

7 Acknowledgments

The author is grateful to Juan Alonso and Luigi Martinelli for their assistance in assembling the text with LaTeX. This research has benefited greatly from the generous support of the AFOSR under grant number AFOSR-91-0391, ARPA under grant number N00014-92-J-1976, USRA through RIACS, and IBM. The warm hospitality of the Aeronautics and Astronautics Department of Stanford University, and NASA Ames Research Center, provided a very favorable environment for the pursuit of this research while the author was on leave from Princeton University.

References

[1] O. Baysal and M. E. Eleshaky. Aerodynamic design optimization using sensitivity anaysis and computational fluid dynamics. *AIAA paper 91-0471*, 29th Aerospace Sciences Meeting, Reno, Nevada, January 1991.

[2] M.O. Bristeau, O. Pironneau, R. Glowinski, J. Periaux, P. Perrier, and G. Poirier. On the numerical solution of nonlinear problems in fluid dynamics by least squares and finite element methods (II). application to transonic flow simulations. In J. St. Doltsinis, editor, *Proceedings of the 3rd International Conference on Finite Element Methods in Nonlinear Mechanics, FENOMECH 84, Stuttgart, 1984*, pages 363–394, North Holland, 1985.

[3] A. Jameson. Iterative solution of transonic flows over airfoils and wings, including flows at Mach 1. *Communications on Pure and Applied Mathematics*, 27:283–309, 1974.

[4] A. Jameson. Acceleration of transonic potential flow calculations on arbitrary meshes by the multiple grid method. *AIAA paper 79-1458*, Fourth AIAA Computational Fluid Dynamics Conference, Williamsburg, Virginia, July 1979.

[5] A. Jameson. Solution of the Euler equations by a multigrid method. *Applied Mathematics and Computations*, 13:327–356, 1983.

[6] A. Jameson. Multigrid algorithms for compressible flow calculations. In W. Hackbusch and U. Trottenberg, editors, *Lecture Notes in Mathematics, Vol. 1228*, pages 166–201. Proceedings of the 2nd European Conference on Multigrid Methods, Cologne, 1985, Springer-Verlag, 1986.

[7] A. Jameson. Aerodynamic design via control theory. *Journal of Scientific Computing*, 3:233–260, 1988.

[8] A. Jameson. Automatic design of transonic airfoils to reduce the shock induced pressure drag. In *Proceedings of the 31st Israel Annual Conference on Aviation and Aeronautics, Tel Aviv*, pages 5–17, February 1990.

[9] A. Jameson. Artificial diffusion, upwind biasing, limiters and their effect on accuracy and multigrid convergence in transonic and hypersonic flows. *AIAA paper 93-3359*, AIAA 11th Computational Fluid Dynamics Conference, Orlando, Florida, July 1993.

[10] A. Jameson. Optimum aerodynamic design via boundary control. Technical report, AGARD FDP/Von Karman Institute Special Course on Optimum Design Methods in Aerodynamics, Brussels, April 1994.

[11] M.J. Lighthill. A new method of two-dimensional aerodynamic design. *R & M 1111*, Aeronautical Research Council, 1945.

[12] J.L. Lions. *Optimal Control of Systems Governed by Partial Differential Equations.* Springer-Verlag, New York, 1971. Translated by S.K. Mitter.

[13] O. Pironneau. *Optimal Shape Design for Elliptic Systems.* Springer-Verlag, New York, 1984.

[14] J. Reuther and A. Jameson. Control theory based airfoil design for potential flow and a finite volume discretization. *AIAA paper 91-499*, 32th Aerospace Sciences Meeting and Exibit, Reno, Nevada, January 1994.

[15] J. Reuther and A. Jameson. Aerodynamic shape optimization of wing and wing-body configurations using control theory. *AIAA paper 95-0213*, 33rd Aerospace Sciences Meeting and Exibit, Reno, Nevada, January 1995.

[16] S. Ta'asan, G. Kuruvila, and M. D. Salas. Aerodynamic design and optimization in one shot. *AIAA paper 91-005*, 30th Aerospace Sciences Meeting and Exibit, Reno, Nevada, January 1992.

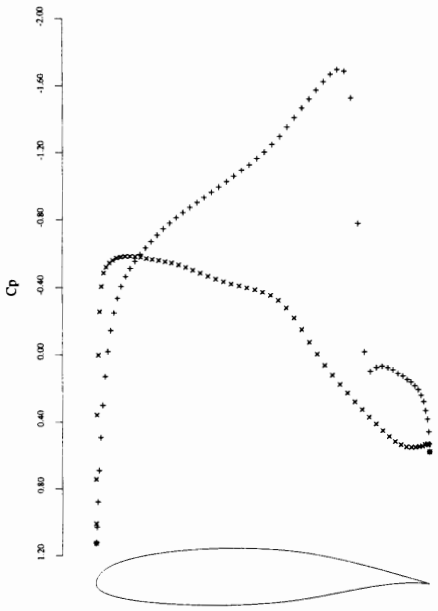

3a: C_p after Zero Design Cycles.
Design Mach 0.72, $C_l = 0.5982$, $C_d = 0.0191$.

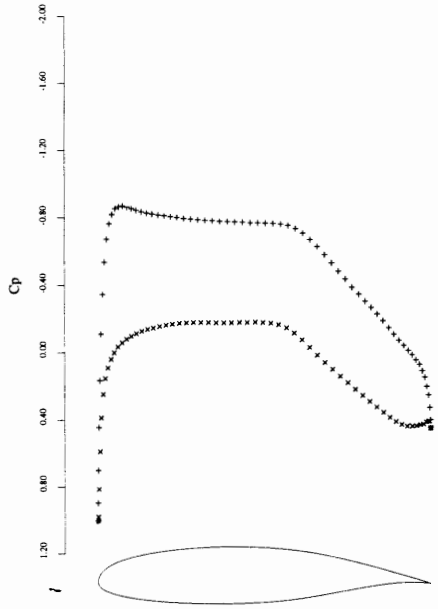

3b: C_p after Zero Design Cycles.
Design Mach 0.2, $C_l = 0.5998$, $C_d = -0.0001$.

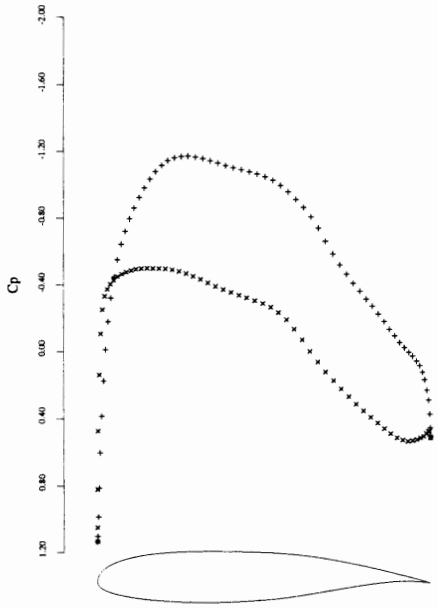

3c: C_p after Eight Design Cycles.
Design Mach 0.72, $C_l = 0.5999$, $C_d = 0.0001$.

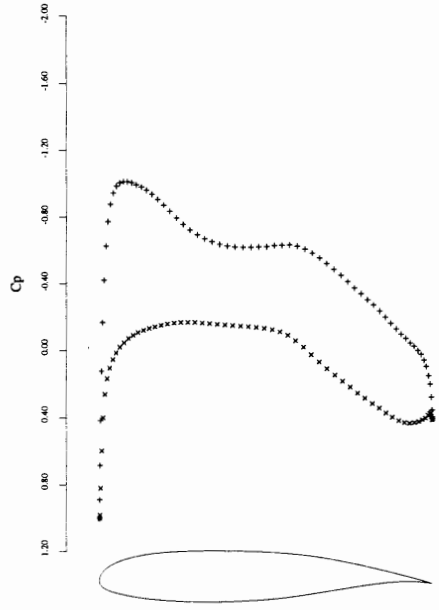

3d: C_p after Eight Design Cycles.
Design Mach 0.2, $C_l = 0.5998$, $C_d = -0.0001$.

Figure 3: Optimization of an Airfoil at Two Design Points.

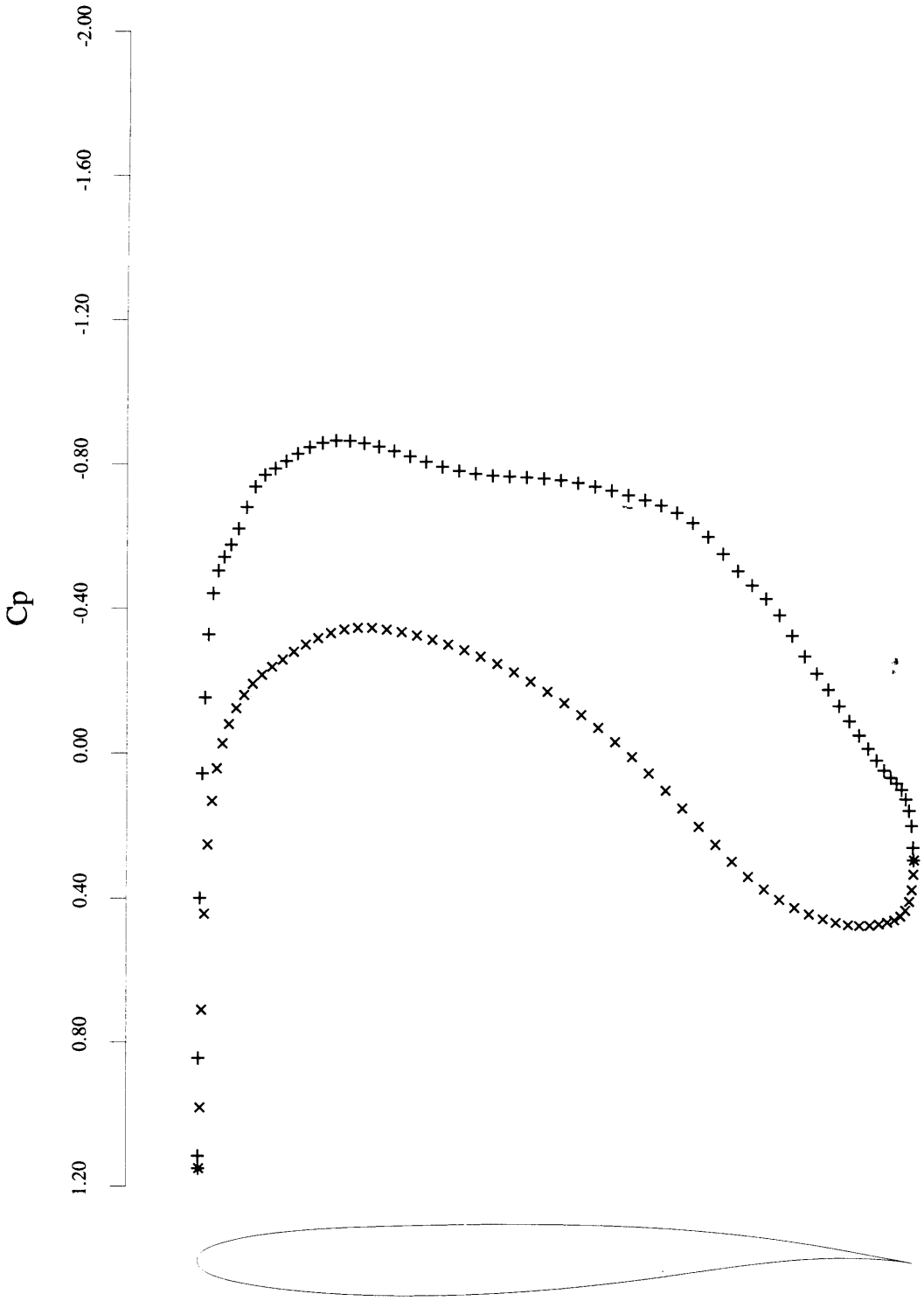

Figure 4: Initial Wing Section and Target Pressure Distribution

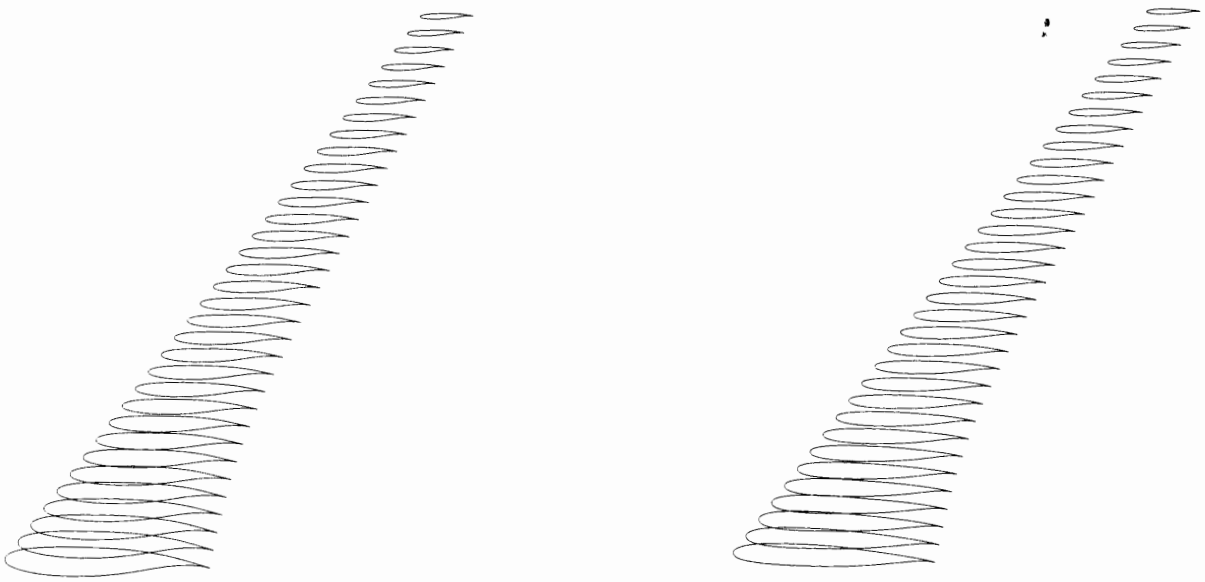

5a: Initial Wing
$C_l = 0.5001$, $C_d = 0.0207$, $\alpha = -1.340°$

5b: 40 Design Iterations
$C_l = 0.5000$, $C_d = 0.0113$, $\alpha = -.235°$

Figure 5: Lifting Design Case, $M = 0.85$, Fixed Lift Mode.
Drag Reduction

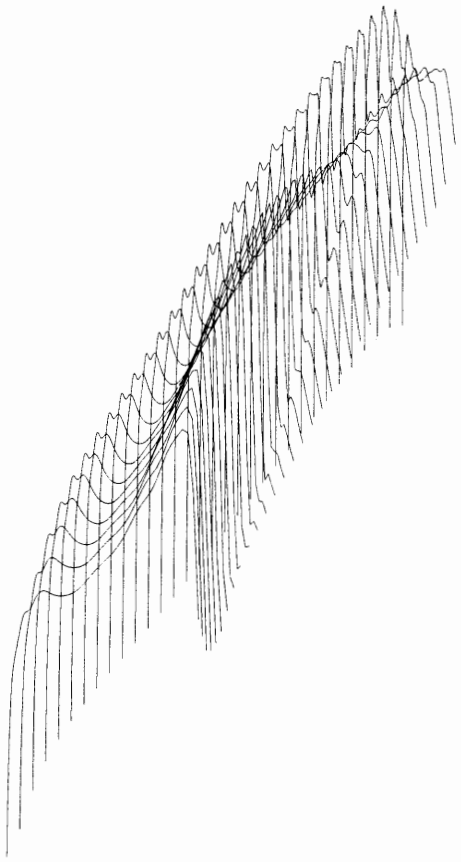

UPPER SURFACE PRESSURE

6a: Initial Wing
Lifting Design Case, $M = 0.85$, Fixed Lift Mode.
$C_L = 0.5001$, $C_D = 0.0207$, $\alpha = -1.340°$
Drag Reduction

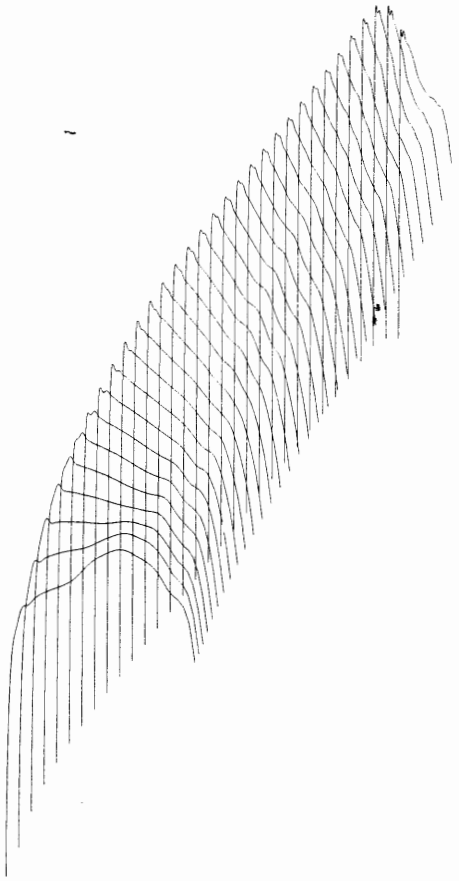

UPPER SURFACE PRESSURE

6b: 40 Design Iterations
Lifting Design Case, $M = 0.85$, Fixed Lift Mode.
$C_L = 0.5000$, $C_D = 0.0113$, $\alpha = -0.235°$
Drag Reduction

Figure 6: Lifting Design Case, $M = 0.85$, Fixed Lift Mode.
Drag Reduction

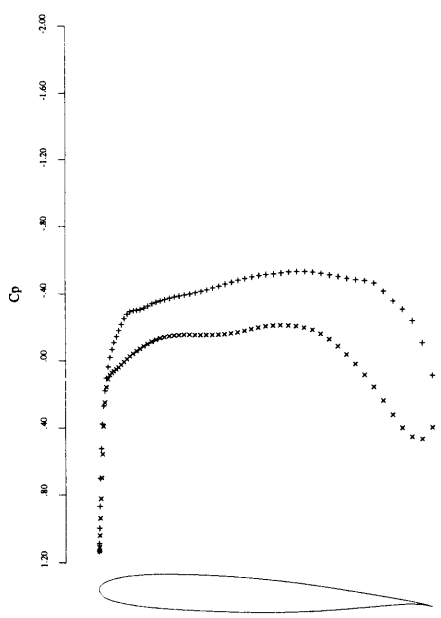

7a: span station $z = 0.00$

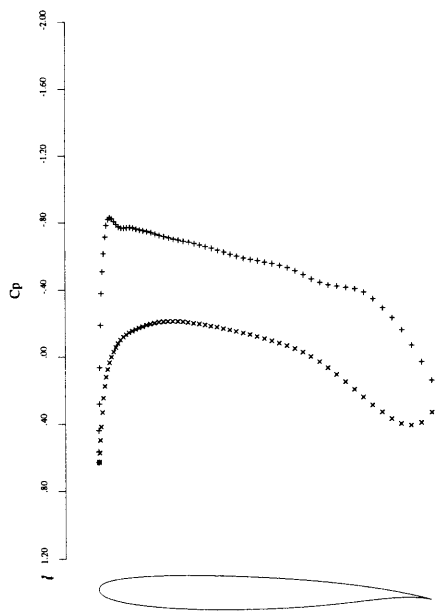

7b: span station $z = 0.312$

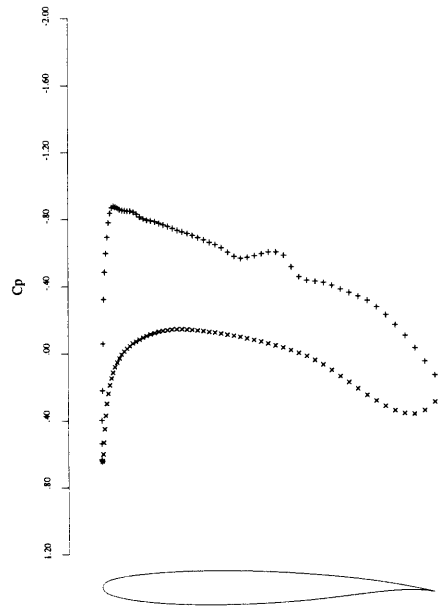

7c: span station $z = 0.625$

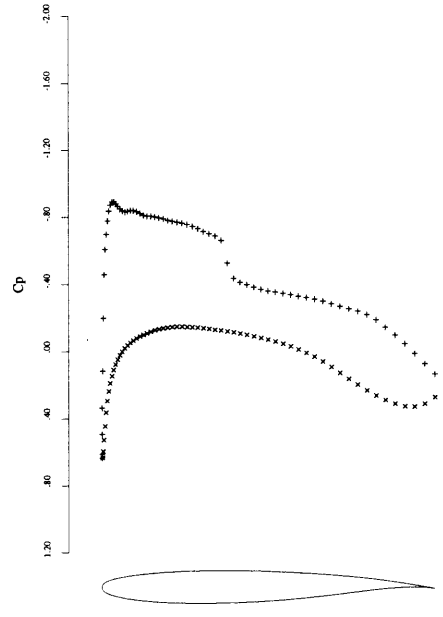

7d: span station $z = 0.937$

Figure 7: FLO67 check on redesigned wing.
$M = 0.85$, $C_L = 0.4977$, $C_D = 0.0094$, $\alpha = -.240°$.

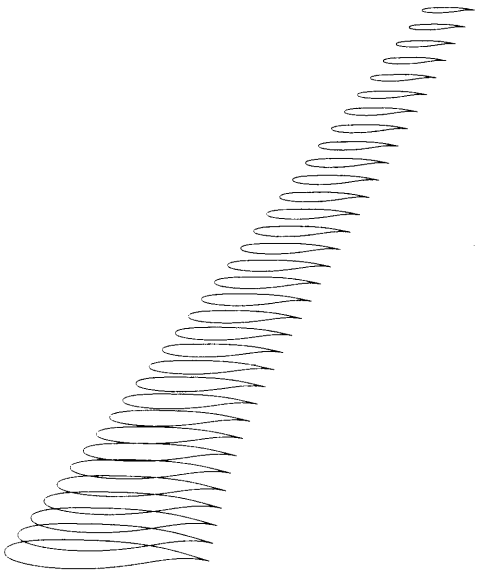

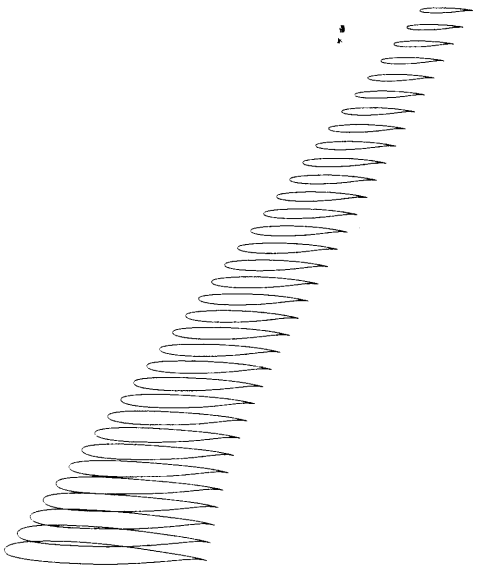

8a: Initial Wing
$C_l = 0.5500$, $C_d = 0.0241$, $\alpha = -0.954°$

8b: 48 Design Iterations
$C_l = 0.5500$, $C_d = 0.0136$, $\alpha = 0.190°$

Figure 8: Lifting Design Case, $M = 0.85$, Fixed Lift Mode.
Drag Reduction

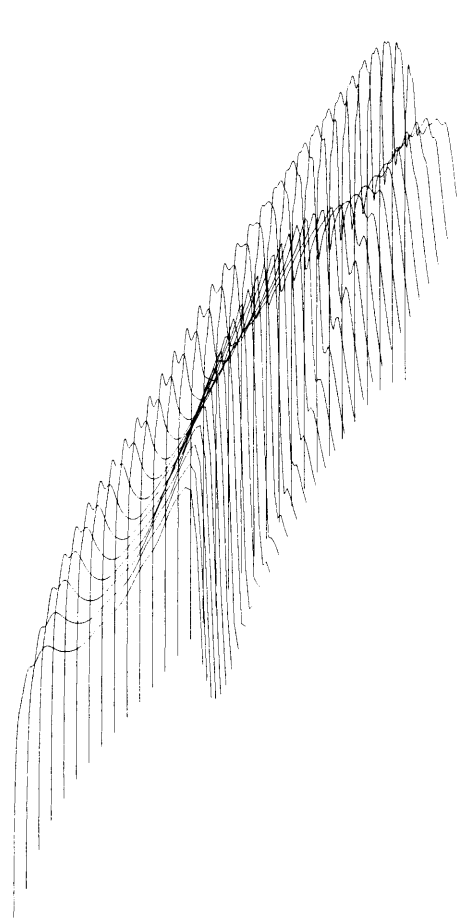

UPPER SURFACE PRESSURE

9a: Initial Wing
Lifting Design Case, $M = 0.85$, Fixed Lift Mode.
$C_L = 0.5500$, $C_D = 0.0241$, $\alpha = -0.954°$
Drag Reduction

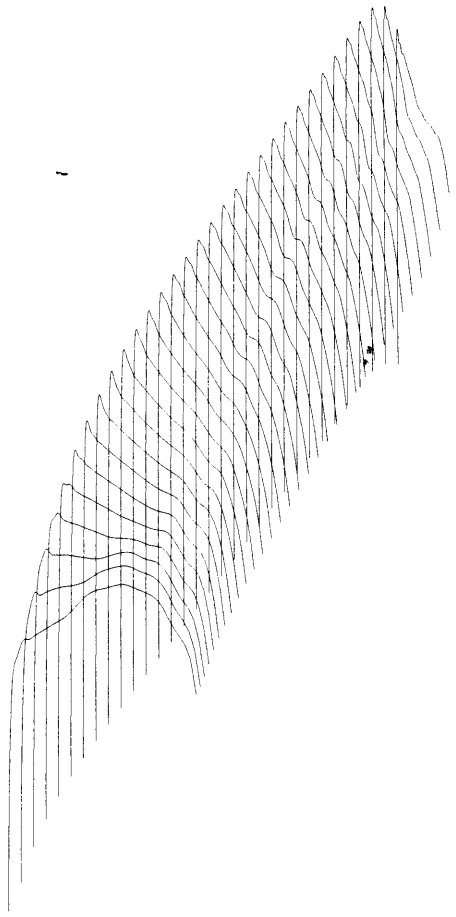

UPPER SURFACE PRESSURE

9b: 10 Design Iterations
Lifting Design Case, $M = 0.85$, Fixed Lift Mode.
$C_L = 0.5500$, $C_D = 0.0136$, $\alpha = 0.190°$
Drag Reduction

Figure 9: Lifting Design Case, $M = 0.85$, Fixed Lift Mode.
Drag Reduction

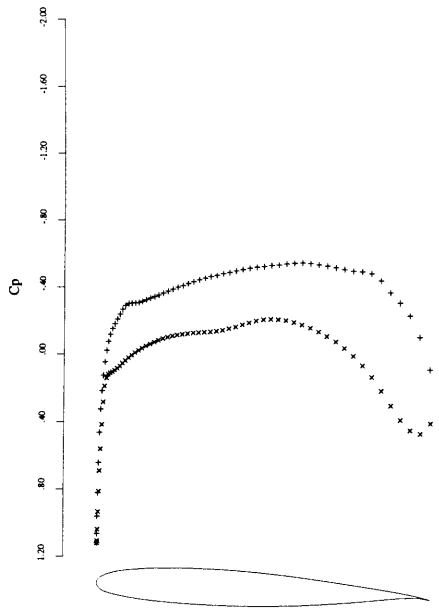

10a: span station $z = 0.00$

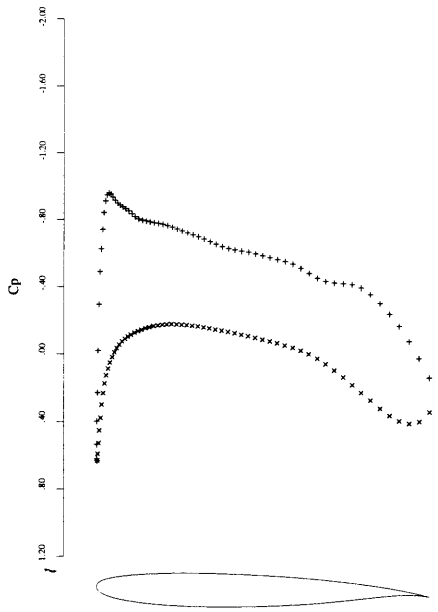

10b: span station $z = 0.312$

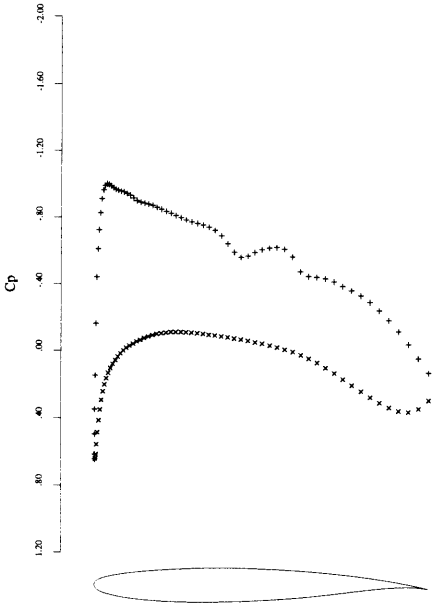

10c: span station $z = 0.625$

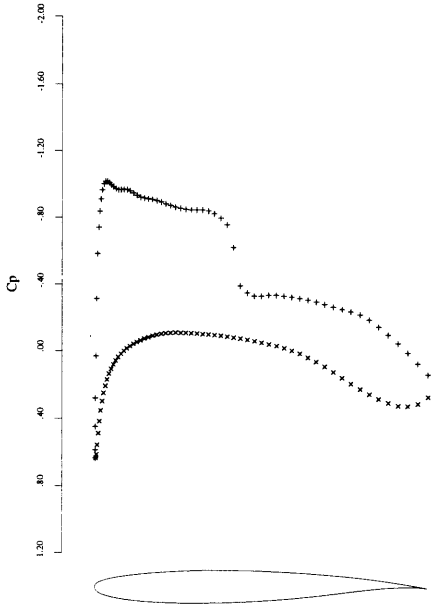

10d: span station $z = 0.937$

Figure 10: FLO67 check on redesigned wing.
$M = 0.85$, $C_L = 0.5491$, $C_D = 0.0115$, $\alpha = 0.190°$.

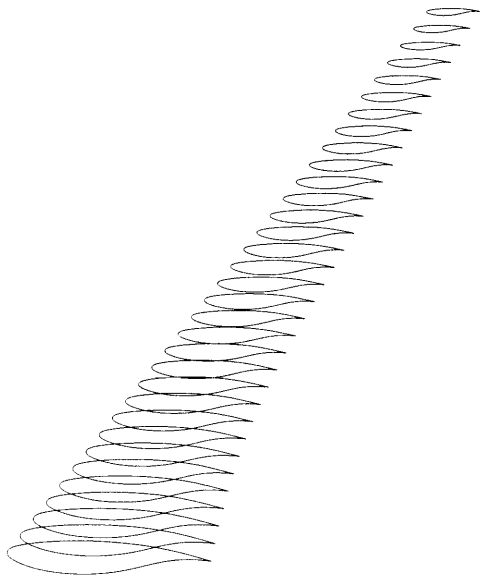

11a: Initial Wing
$C_l = 0.5001$, $C_d = 0.0253$, $\alpha = 0.063°$

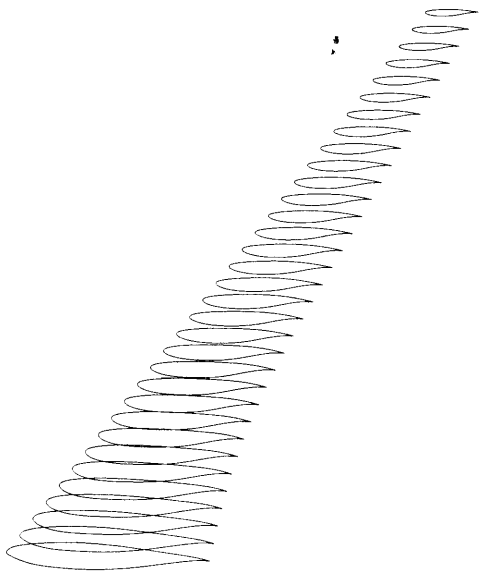

11b: 48 Design Iterations
$C_l = 0.5000$, $C_d = 0.0118$, $\alpha = 0.595°$

Figure 11: Lifting Design Case, $M = 0.85$, Fixed Lift Mode.
Drag Reduction

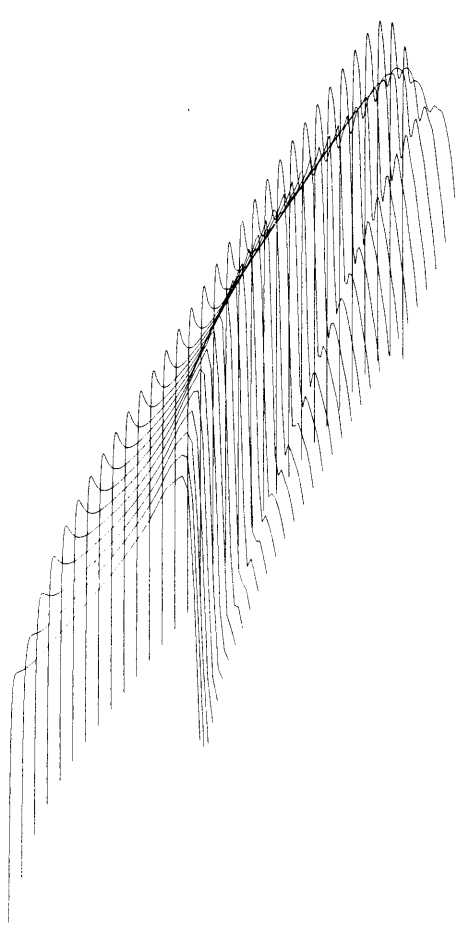

UPPER SURFACE PRESSURE

12a: Initial Wing
Lifting Design Case, $M = 0.85$, Fixed Lift Mode.
$C_L = 0.5001$, $C_D = 0.0253$, $\alpha = 0.063°$
Drag Reduction

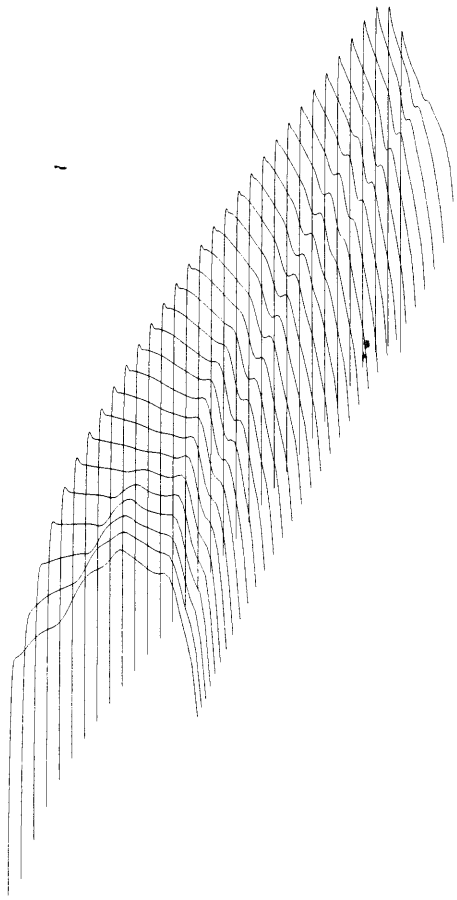

UPPER SURFACE PRESSURE

12b: 48 Design Iterations
Lifting Design Case, $M = 0.85$, Fixed Lift Mode.
$C_L = 0.5500$, $C_D = 0.0118$, $\alpha = 0.595°$
Drag Reduction

Figure 12: Lifting Design Case, $M = 0.85$, Fixed Lift Mode.
Drag Reduction

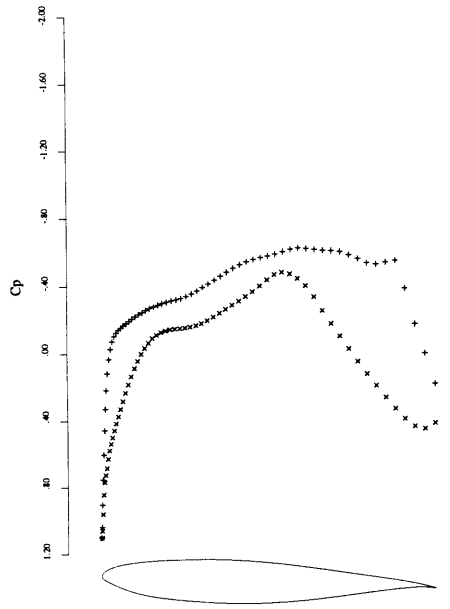

13a: span station $z = 0.00$

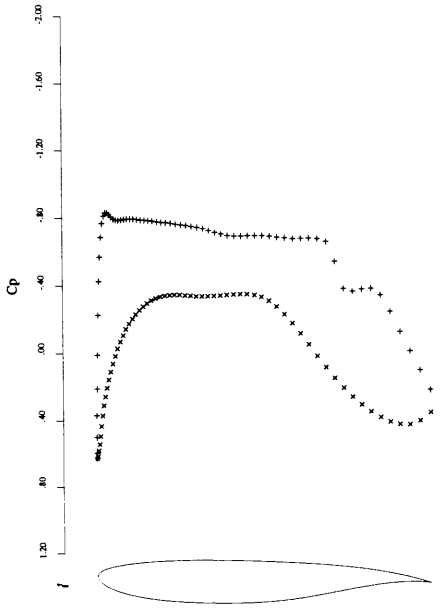

13b: span station $z = 0.312$

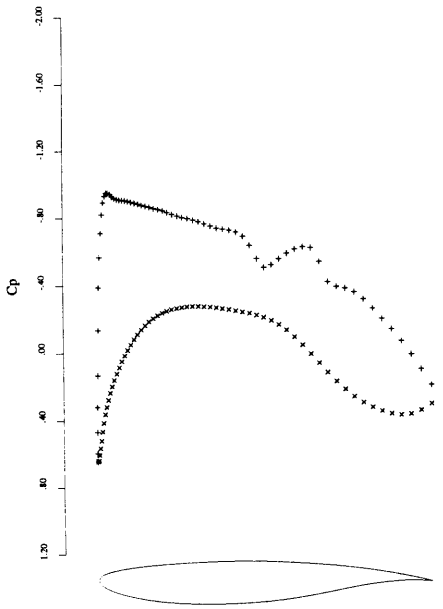

13c: span station $z = 0.625$

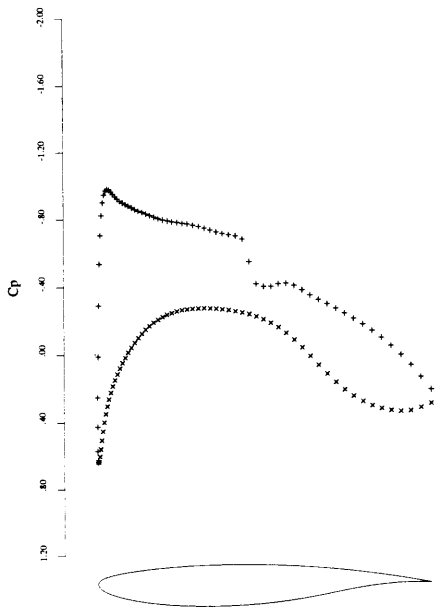

13d: span station $z = 0.937$

Figure 13: FLO67 check on redesigned wing.
$M = 0.85$, $C_L = 0.4994$, $C_D = 0.0099$, $\alpha = 0.590°$.